2-D shapes description by using features based on the differential turning angle scalogram

Kidiyo Kpalma, Mingqiang Yang, Kamel Belloulata

Journal of Pattern Recognition Research 1 (2014) 90-110

Received March 13, 2014. Revised October 10, 2014. Accepted October 05, 2014.

2-D shapes description by using features based on the differential turning angle scalogram

Kidiyo Kpalma *kidiyo.kpalma@insa-rennes.fr*
Université Européenne de Bretagne, France - INSA, IETR, UMR 6164, F-35708 RENNES

Mingqiang Yang *yangmq@sdu.edu.cn*
ISE - Shandong University - 250100, Jinan, China

Kamel Belloulata *k_belloula@yahoo.fr*
Electronics Department - University of Djillali Liabes - Sidi bel Abbes, Algeria

Abstract

A 2-D shape description using the turning angle is presented [1]. This descriptor is based on a scalogram obtained from a progressive filtering of a planar closed contour. At a given scale, the differential turning angle function is calculated from which, three essential points are derived: the minimum differential-turning angle (α-points), the maximum differential-turning angle (β-points) and the zero-crossing of the turning angle (γ-points). For a continuum of the scale values in the filtering process, a map (called d-TASS map) is generated. As shown experimentally in a previous study, this map is invariant under rotation, translation and scale change. Moreover, it is shearing and noise resistant. The contribution of the present study is firstly, to prove theoretically that d-TASS is rotation and scale change invariant and secondly to propose a new descriptor extracted from the blocks within the scalogram. When applied to shape retrieval from commonly used image databases like MPEG-7 Core Experiments Shape-1 dataset, Multiview Curve Dataset and marines animals of SQUID dataset, experimental results yield very encouraging efficiency and effectiveness of the new analysis approach and the proposed descriptor.

Keywords: pattern analysis, pattern recognition, turning/tangential angle, multi-scale analysis, scale-space analysis, CBIR

1. Introduction

With the development of the technology, we are facing more and more images that we have to handle and understand. In this context automatic image retrieval from within large databases is necessary: the corresponding system have to integrate a simple, fast and efficient algorithm for shape feature extraction and representation. Petrakis et al. in [3] and Kpalma et al. in [4] present a sample set of criteria for shape representation for reliable shape matching and retrieval. Among these criteria, is the uniqueness, the robustness, the invariance, the scalability, the efficiency, the compactness, the reliability... Uniqueness means that the representation must uniquely describe a shape ; otherwise, a query may retrieve shapes that are not similar to it. The robustness states that the representation must be resistant to distortions and noise, which are typical on natural shapes. The invariance indicates that the representation must be insensitive to viewing conditions that the shape could undergo: it must be invariant to translation, scale change, rotation, and viewing angle. The scalability will help to capture information about the shape at many scales so that similar shapes can be recognized even if they appear at different resolutions. An efficient representation must be computationally efficient. A compact representation uses a low number of features. The

1. This paper is a broad extension of [1] and [2] and its evaluation over various databases.

reliability means that the extracted features remain the same as long as one deals with the same pattern.

d-TASS (differential-Turning Angle Scale Space) function is presented in [1] and [2], and some shape features extracted from it were introduced therein. It was then shown that this scale space representation of planar objects yields characteristic properties that are interesting in the context of shape description. In [2], it has been shown that this representation complies with a number of criteria listed above: it is rotation, translation and scale change invariant and that it is also shearing and noise resistant.

The current paper aims at to demonstrate theoretically that d-TASS scalograms are invariant under rotation and scale change. Then we propose and evaluate new features extracted from these scalograms. The evaluation of the proposal is conducted upon 4 databases and then the retrieval performance based on the bull's eye measure [5] is compared to that provided by well-known state-of-the-art methods.

The rest of the paper is organized as follows: section 2 recalls the principle of the method; it presents the differential turning angle scalogram and defines the d-TASS map. Section 3 concerns the definition of the new descriptor. Section 4 is dedicated to the evaluation of the proposed descriptor. Finally, in section 5, discussions are presented and then the paper is concluded.

2. Differential turning angle scalogram generation

This approach is based on the analysis of closed contours and belongs to the group of contour-based shape representations in accordance with the classification done by Zhang et al. [6]. An input contour is represented by a sequence of points defined by their (x, y) coordinates. First, the input contour is separated into two functions x(u) and y(u) which are functions of a normalized curvilinear parameter u that varies from 0 to 2π relatively to the curve length. Each point of the curve is then represented by its coordinates (x_n, y_n) where $x_n = x(u_n)$ and $y_n = y(u_n)$ are the coordinates corresponding to the sampled curvilinear abscissa. If the number of the points is set to N, then the index n varies from 0 to N-1. In this study, N is set to 360 points reorganized in counter clockwise as explained in [2].

2.1 Differential turning angle: definition

In order to reduce the effect of various deformations that could affect the contour, this one is firstly normalized as proposed in [7] by Avrithis et al. Then, given a starting point P_0, the points are numbered from P_0 to P_{n-1}.

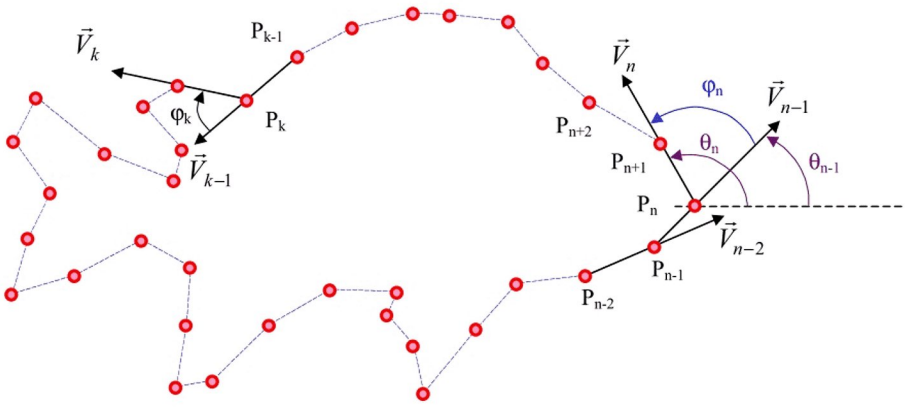

Fig.1: Illustration of the differential-turning angle

Let $\overrightarrow{V}_n$ be the vector defined by the two points P_n and P_{n+1} originating at P_n and oriented towards P_{n+1}. The turning angle θ_n at point P_n is the angle between vector $\overrightarrow{V}_n$ and the x-axis. Figure 1, illustrates the principle. The differential-Turning Angle (d-TA) function is the angle φ_n between two consecutive vectors $\overrightarrow{V}_{n-1}$ and $\overrightarrow{V}_n$; in other words:

$$\varphi_n = \theta_n - \theta_{n-1} \tag{1}$$

2.2 Differential turning angle: scalogram construction

Fig.2 shows an example of the d-TA function. The parts of the contour pointed by letters from (a) to (k) are represented by specific behavior on the d-TA function as demonstrated by the letters (A) through (K).

From the d-TA function, a scalogram is generated: we call it the differential-Turning Angle Scale Space (d-TASS) function. To generate the d-TASS function, the input contour is progressively smoothened with a Gaussian filter by reducing its bandwidth as proposed in [1] and [8].

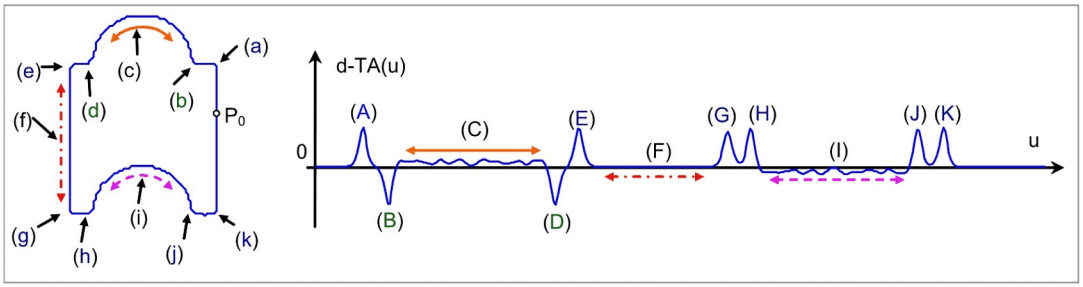

Fig.2: Example of a contour and its d-TA function at a given scale.

For a given Gaussian kernel, we obtain progressive filtering by iterating the operation. By doing so, the filtering scale σ_n is reached after n iterations so that $\sigma_n = \sigma_0\sqrt{n}$ where σ_0 is the standard deviation of the Gaussian kernel. In this study, the Gaussian kernel of size 3, g=[0.25, 0.50, 0.25], corresponding to $\sigma_0 = \sqrt{2/\pi}$ is used. Based on this d-TASS function, three essential points are derived to give the d-TASS map (see [4]); the definition of the essential points, is as follows:

- α-points are those with a local minimum of d-TASS function (green on Fig.4),
- β-points are those with a local maximum of d-TASS function (blue on Fig.4)
- γ-points are those that correspond to the zero-crossing of the d-TASS function (red on Fig.4).

Figure 3 illustrates the procedure generating the d-TASS map. Starting from the input coordinates sequences X_0=x and Y_0=y, the d-TA function is computed to generate corresponding essential points. When an essential point is detected at a given location, this location is marked "1" in the corresponding channel (red, green or blue) otherwise, it is marked "0".

As can be seen on the flowchart, prior to the filtering procedure, the contour is resampled by using the so called iso-area normalization [9] so that each input contour have 360 points as explained in [8]. The stop condition of the iteration is that "there is no more γ-points at the current scale". Figure 4 shows two examples of d-TASS map on which the x-axis corresponds to the normalized curvilinear abscissa u representing the space variable and the y-axis is related to the scale variable σ. Row n on the map holds the trace of the essential points at the n^{th} iteration.

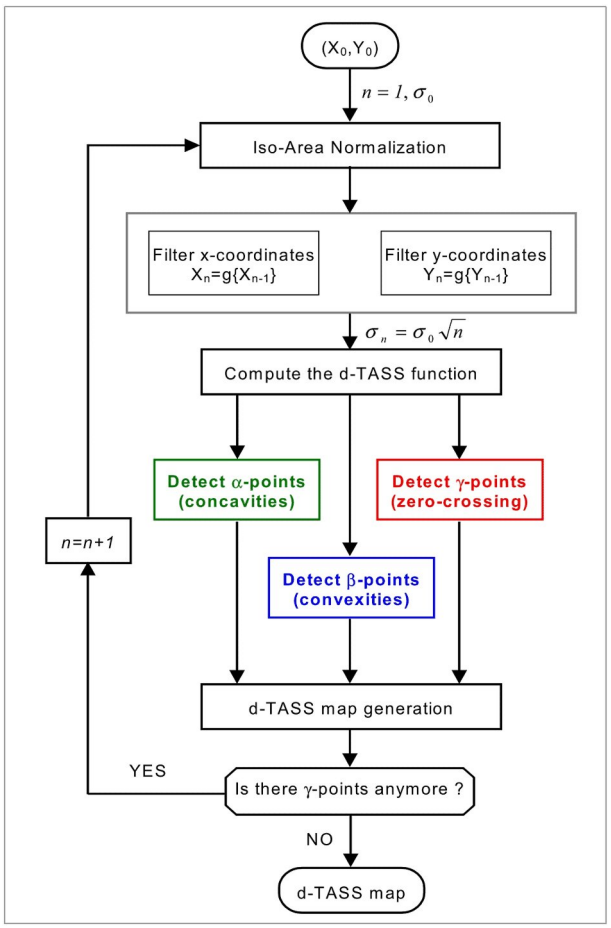

Fig.3: Principle of d-TASS generation

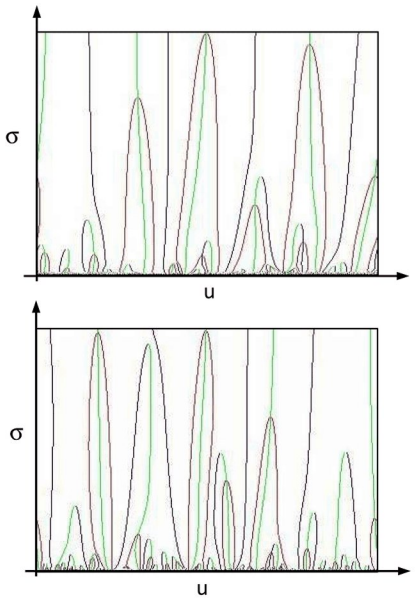

Fig.4: Examples of d-TASS map

To compensate for rotation, a circular translation of the d-TASS map is performed before extracting features. This translation is done so that the maximum peak of γ-points in the map is aligned on the abscissa value of 180 (see Fig.4). Figure 5 shows a set of contours obtained from a contour after it has undergone a transformation of equation (16) with various values of the transformation parameters (θ, h, λ) representing respectively, the rotation angle, the scale factor and the shearing factor.

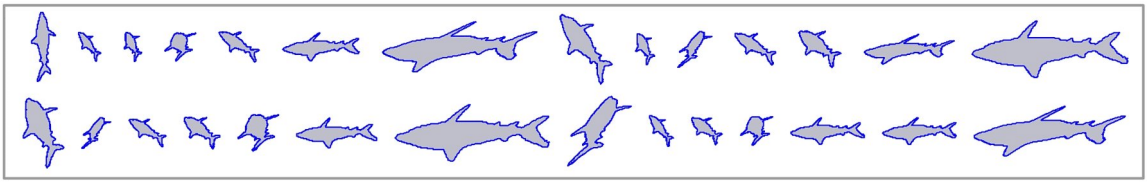

Fig.5: Example of a contour and its affine transforms.

The corresponding d-TASS maps are represented on Fig.6: as it can be seen, these maps are visually similar. This confirms that the d-TASS map is representative of the contour and that it is robust and invariant under various transformations.

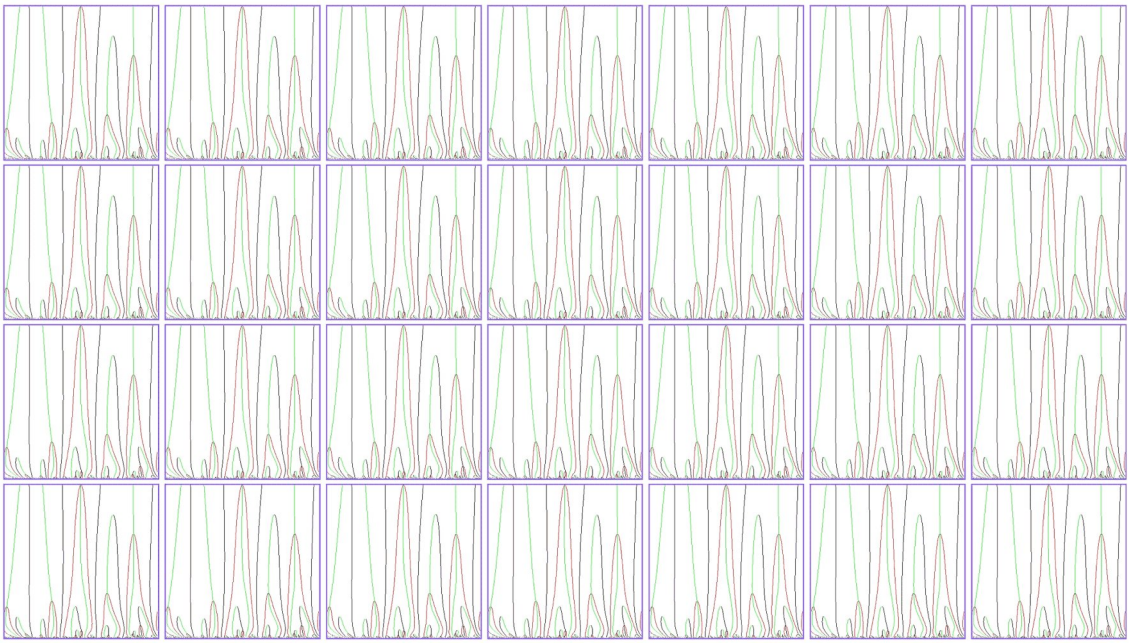

Fig.6: d-TASS maps of the contours in figure 5

2.3 d-TASS vs. affine transforms

In this section, we demonstrate the effect of an affine transform on the d-TASS. First, we will consider a general affine transformation and then we will analyze the particular cases of rotation and scaling. Let A be the affine transform matrix and $\vec{T}$ the translation vector of coordinates T_x and T_y. The matrix is defined by four real-valued parameters a, b, c and d as follows:

$$A = \begin{pmatrix} a & b \\ c & d \end{pmatrix} \tag{2}$$

A given point P of coordinates P(x,y) is then transformed onto the point P'(x',y'):

$$\begin{pmatrix} x' \\ y' \end{pmatrix} = \begin{pmatrix} a & b \\ c & d \end{pmatrix} \begin{pmatrix} x \\ y \end{pmatrix} + \vec{T} = \begin{pmatrix} \mathrm{ax} + \mathrm{by} + T_x \\ \mathrm{cx} + \mathrm{dy} + T_y \end{pmatrix} \tag{3}$$

Let us consider a line segment $(P_n P_{n+1})$ defined by the two points $P_n(x_n, y_n)$ and $P_{n+1}(x_{n+1}, y_{n+1})$ (see figure 7). The angle θ_n between this segment and the x-axis is defined by:

$$\theta_n = \mathrm{arctg}\left(\frac{y_{n+1} - y_n}{x_{n+1} - x_n}\right) \tag{4}$$

d-TASS vs. translation: now suppose that this segment has undergone an affine transformation as defined by equation (3). The angle between the transformed segment $(P'_n P'_{n+1})$ and the x-axis is given by:

$$\theta'_n = \mathrm{arctg}\left(\frac{y'_{n+1} - y'_n}{x'_{n+1} - x'_n}\right) = \mathrm{arctg}\left(\frac{c(x_{n+1} - x_n) + d(y_{n+1} - y_n)}{a(x_{n+1} - x_n) + b(y_{n+1} - y_n)}\right)$$

From this relation, it is clear that the turning angle θ'_n never depends on the translation: the turning angle is invariant under any translation.

By rearranging this expression, we obtain

$$\theta'_n = \text{arctg}\left(\frac{\frac{c}{a} + \frac{d}{a}\left(\frac{y_{n+1}-y_n}{x_{n+1}-x_n}\right)}{1 + \frac{b}{a}\left(\frac{y_{n+1}-y_n}{x_{n+1}-x_n}\right)}\right) \tag{5}$$

Regarding equation (4), θ'_n can be rewritten as follows:

$$\theta'_n = \text{arctg}\left(\frac{\frac{c}{a} + \frac{d}{a}\text{tg}(\theta_n)}{1 + \frac{b}{a}\text{tg}(\theta_n)}\right) \tag{6}$$

In terms of d-TA, the differential angle φ'_n at the point P'_n of the transformed contour is given by the difference of the two angles θ'_n and θ'_{n-1} so that we can write:

$$\varphi'_n = \theta'_n - \theta'_{n-1} = \text{arctg}\left(\frac{\frac{c}{a} + \frac{d}{a}\text{tg}(\theta_n)}{1 + \frac{b}{a}\text{tg}(\theta_n)}\right) - \text{arctg}\left(\frac{\frac{c}{a} + \frac{d}{a}\text{tg}(\theta_{n-1})}{1 + \frac{b}{a}\text{tg}(\theta_{n-1})}\right) \tag{7}$$

By definition, the φ'_n angle is the angle between two line segments: one from point P'_{n-1} to point P'_n and the other from P'_n to P'_{n+1} as illustrated on the following figure. On Fig.7(a), one can observe that the angle between line segments $(P_{n-1}P_n)$ and (P_nP_{n+1}) is φ_n. Fig.7(b) corresponds to the rotation of Fig.7(a) through angle θ around the origin. As can be observed, the angle between line segments $(P'_{n-1}P'_n)$ and $(P'_nP'_{n+1})$ is also φ_n. This will be proved below.

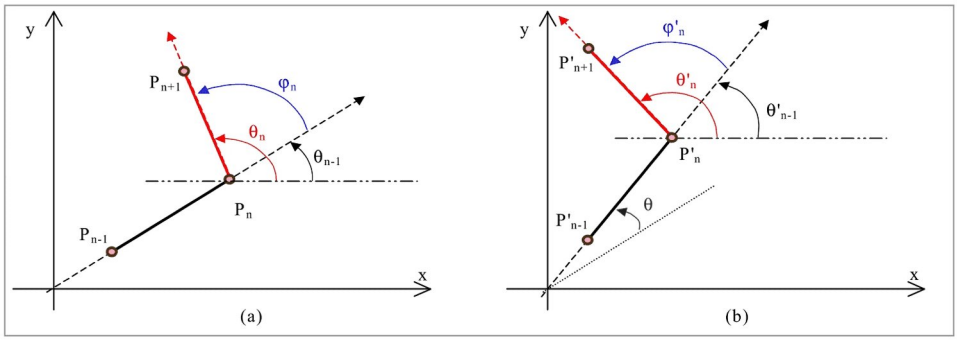

Fig.7: The differential turning angle face to rotation

For convenience and simplicity of the analysis, let's calculate the tangent of φ'_n based on the following relation for two angles α and β

$$\text{tg}(\alpha - \beta) = \frac{\text{tg}(\alpha) - \text{tg}(\beta)}{1 + \text{tg}(\alpha)\text{tg}(\beta)} \tag{8}$$

equation (7) rewrites as follows:

$$\text{tg}(\varphi'_n) = \left(\frac{\frac{c}{a} + \frac{d}{a}\text{tg}(\theta_n)}{1 + \frac{b}{a}\text{tg}(\theta_n)} - \frac{\frac{c}{a} + \frac{d}{a}\text{tg}(\theta_{n-1})}{1 + \frac{b}{a}\text{tg}(\theta_{n-1})}\right) / \left(1 + \frac{\frac{c}{a} + \frac{d}{a}\text{tg}(\theta_n)}{1 + \frac{b}{a}\text{tg}(\theta_n)} \times \frac{\frac{c}{a} + \frac{d}{a}\text{tg}(\theta_{n-1})}{1 + \frac{b}{a}\text{tg}(\theta_{n-1})}\right) \tag{9}$$

Equation (9) linking a general affine transform to the differential turning angle shows that d-TASS is not invariant under general affine transform. But starting from this relation, one can prove the invariance for two particular cases that are scaling and rotation.

d-TASS vs. scaling: in the case of a simple scaling, the transformation matrix is defined by: b=c=0 and a=d then the previous relation (9) becomes:

$$\mathrm{tg}(\varphi'_n) = \frac{\mathrm{tg}(\theta_n) - \mathrm{tg}(\theta_{n-1})}{1 + \mathrm{tg}(\theta_n)\mathrm{tg}(\theta_{n-1})} = \mathrm{tg}(\theta_n - \theta_{n-1}) = \mathrm{tg}(\varphi_n)$$

From this, it appears that $\varphi'_n = \varphi_n$ proving that d-TASS is invariant under scaling.
d-TASS vs. rotation: when concerned by a rotation through angle θ (see Figure 7) around the origin, the transformation matrix becomes a=d= cos(θ) and b=-c= sin(θ). By proceeding as previously, equation (9) becomes:

$$\mathrm{tg}(\varphi'_n) = \frac{\mathrm{tg}(\theta + \theta_n) - \mathrm{tg}(\theta + \theta_{n-1})}{1 + \mathrm{tg}(\theta + \theta_n) \times \mathrm{tg}(\theta + \theta_{n-1})} = \mathrm{tg}(\theta_n - \theta_{n-1}) = \mathrm{tg}(\varphi_n)$$

Again, it is clear that $\varphi'_n = \varphi_n$ indicating that d-TASS is invariant under rotation. Based on these properties, a new descriptor is proposed for contour characterization.

3. Proposed descriptor and pattern description

3.1 Combination of essential points

For pattern description, we propose a feature matrix based on weighted moments of the content of blocks within the d-TASS map. First, d-TASS maps are cut up into R rows by C columns blocks: hence each block is referred to by using its coordinates r (r=1, 2, ..., R) and c (c=1, 2, ..., C). These blocks are considered to be possibly overlapping as illustrated on figure 9. Typically, 25% overlapping is found to be the most performing. For a given block located at (r,c), let B^{α}_{rc}, B^{β}_{rc}, and B^{γ}_{rc} be the corresponding blocks from α, β and γ essential points, respectively. From these blocks, we generate the block B_{rc}, defined by:

$$B_{\mathrm{rc}} = w_\alpha B^{\alpha}_{\mathrm{rc}} + w_\beta B^{\beta}_{\mathrm{rc}} + w_\gamma B^{\gamma}_{\mathrm{rc}} \tag{10}$$

where w_α, w_β and w_γ are the weights applied, respectively, to α-, β- and γ-points. In other words, B_{rc} is obtained by using a pixel-wise linear combination of the blocks of the three essential points maps: $B_{\mathrm{rc}}(m,n) = w_\alpha B^{\alpha}_{\mathrm{rc}}(m,n) + w_\beta B^{\beta}_{\mathrm{rc}}(m,n) + w_\gamma B^{\gamma}_{\mathrm{rc}}(m,n)$, for pixel (m,n). Each pixel containing an essential point is supposed to be unity and null otherwise.

3.2 Matrix-wise descriptor

From this B_{rc} block, we compute the corresponding coefficient M_{pq}(r,c) as follows:

$$M_{\mathrm{pq}}(r,c) = m_{\mathrm{pq}} \tag{11}$$

where p=0 or 1 and q=0 or 1. The coefficient M_{pq}(r,c) is an element of the feature matrix M_{pq} and m_{pq} represents the first three moments (m_{00}, m_{01} and m_{10}) of the B_{rc} block. Jointly with these moments, we define and use the mean value M_0 of the inter-essential points distance. The following figure illustrates the principle of the inter-essential points distance measurement at a given scale.

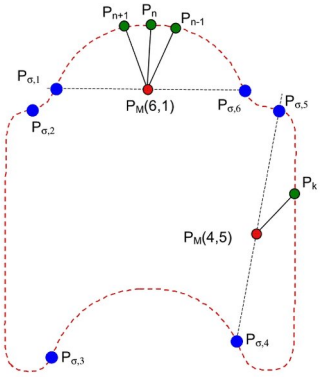

Fig.8: Definition of the inter-essential points distance

The inter-essential points distance function is the distance between the current contour point P_n and the mid-point P_M(s,t) between the two consecutive γ-points $P_{\sigma,s}$ and $P_{\sigma,t}$. As for illustration, figure 8 shows six γ-points ($P_{\sigma,1}$, $P_{\sigma,2}$,..., $P_{\sigma,6}$). P_M(6,1) represents the mid-point between the consecutive γ-points $P_{\sigma,6}$ and $P_{\sigma,1}$. By iterating the process for a range of scales (until the stop condition), we obtain the distance scale space function (DSSF).

Figure 9 illustrates the principle of blocks creation and feature matrix generation: Fig.9.a) represents the gridding applied to the d-TASS map and Fig.9.b) shows an illustration of the resulting feature matrix (represented as an image). On Fig.9.c), one can see an example of d-TASS map and, from left to right, the corresponding M_{00}, M_{01}, M_{10} and M_0 matrices. In this representation, the color demonstrates the value of the moment computed from the corresponding block B_{rc}.

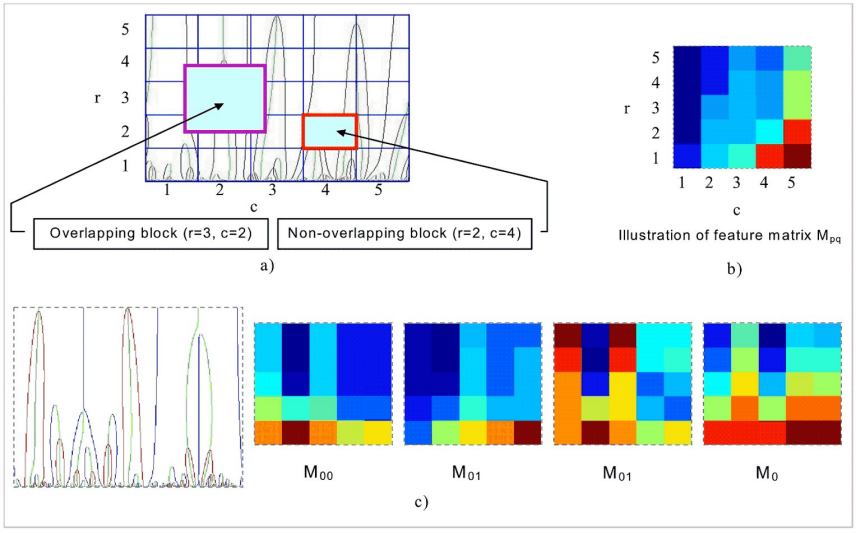

Fig.9: d-TASS-based descriptor construction: a) blocks definition on the d-TASS map, b) corresponding feature matrix, c) example of d-TASS map and, from left to right, its M_{00}, M_{01}, M_{10}, M_0 matrices.

The motivation of using these moments is illustrated on Fig.10 that shows a sample set of typical patterns encountered in B_{rc} blocks. In each block, we have exactly the same number of pixels (in black) with value 1 on a white background (of value zero). As can be seen in Table I, m_{00} is the same for the four patterns. m_{01} and m_{10} are different from a pattern to another so they are likely to carry some discriminating information other than that of m_{00} coefficient.

Fig.10: Examples of typical patterns in B_{rc} blocks of a d-TASS map

Table I: Moments computed from blocks in figure 10.

	m_{00}	m_{10}	m_{01}
I_1	32	272	272
I_2	32	272	270
I_3	32	272	272
I_4	32	296	208

3.3 Similarity measurement

In accordance with the study presented in [10], we have used the Manhattan distance to measure the similarity between two shapes. The similarity between two shapes A and B is the weighted sum of distances computed individually from the moments. Equation (12) gives the definition of the distance between feature matrices M_ω^A and M_ω^B with $\omega = \{00, 01, 10, 0\}$.

$$d_\omega(A, B) = \sum_\omega |M_\omega^A(r, c) - M_\omega^B(r, c)| \tag{12}$$

The global distance is then defined by the following equation (13) where a_ω indicates the weight of the contribution of the distance d_ω.

$$d(A, B) = \sum_\omega \frac{a_\omega d_\omega(A, B)}{1 + \mathrm{SC}_\omega(A) + \mathrm{SC}_\omega(B)} \tag{13}$$

Because features are of different nature and different ranges, it is necessary to normalize their individual distances before these ones can be combined together. For this purpose, we use the shape complexity ; as explained in [11] and [12], the shape complexity with respect to a shape feature is some measure of the extent of this feature. In this study, this measure is defined as $\mathrm{SC}(A) = |\max(V_A) - \min(V_A)|$ where V_A is the feature vector of shape A.

4. Evaluation of the proposed descriptor

The evaluation of the proposed descriptor is based on the comparison of its retrieval results with those obtained from other studies, of the literature such as MCC (Multi-scale Convexity Concavity) [13], TA (Triangle Area) using DSW (Dynamic Space Warping) [11], BAS (Beam Angle Statistics) [14], method presented by Bandera et al. [15], WARP [16], SC (Shape Context) [17], Wavelet [18], ZM (Zernike Moments) [19], TS (Tangent Space) [20], VP (Visual Parts) [21], DAG (Directed Acyclic Graphs) [22], IDSC (Inner Distance Shape Context) [23], CSS (Curvature Scale Space) [24], [25], [26], CED (Curve Edit Distance) [27]. For more details about each method one may consider to have a look at the appropriate reference. To have effective comparison results, the experiments are conducted on five different datasets with more or less complexities in the deformations.

The MCC uses the degree of convexity/concavity at various scale levels as a descriptor. The matching of two contours is then achieved using dynamic programming which provides the dissimilarity measure. The TA-DSW retrieval method uses triangle-area to represent non-rigid shapes based on their closed contours. This measures the convexity/concavity of each point at various scales. The similarity measurement is based on a dynamic space warping (DSW) algorithm that searches for the optimal correspondence between the points of two shapes. The BAS descriptor is based on the beams originating from a boundary point, which are de ?ned as lines connecting that point with the rest of the points on the boundary. The angle between a pair of beams gives a measure of the topological structure of the boundary. The similarity between two shapes is measured by the optimal correspondent subsequence (OCS) algorithm. The method proposed by Bandera et al. is based on a global incremental scheme which combines two learning mechanisms: the Incremental Non-parametric Discriminant Analysis and the mode analysis method. Then feature selection is performed based on an adaptive curvature estimator. The matching of two shapes is then performed by using the incremental mode analysis followed by the k-nearest neighbor classification. WARP is a shape retrieval approach that uses the phase of Fourier coefficients and the similarity between shapes is performed using the Dynamic Time Warping. The SC-based descriptor uses the so called shape context at each point of the contour to determine the corresponding

point. From the corresponding points, the transformation that better aligns the two countours is estimated by using the regularized thin-plate splines and the similarity is obtained by the sum of the matching errors.

The ZM-based shape descriptor consists of the coefficients of Zernike moments. For similarity measure, the nearest-neigbour classification and the minimum-mean-distance are performed. The IDSC descriptor is based on the inner-distance between control points. A dynamic programming based method is then used for shape matching. The CSS descriptor consists of the maxima of curvature zero crossing contours of curvature scale space image and its aspect ratio combined with the eccentricity and the circularity of the contour. The CED retrieval approach is based on the correspondence between two contours. The similarity measure is given by the two intrinsic properties of the contour alignment, namely, length and curvature by using a dynamic-programming method both for aligning pairs of contours segments and pairs of closed contours.

For more details about the differents methods, the reader is urged to refer to the corresponding literature refered herein.

4.1 Description of the experimental datasets

The first dataset is based on the Shape Queries Using Image Databases (SQUID) [28] provided by F. Mokhtarian et al. It is generated by applying affine transformation (rotation, scaling and shearing) to some contours of SQUID database. This enabled us to evaluate the proposed descriptor on a "synthetic" database. This dataset will be referred to as Dataset-I (see Fig.11 and Fig.12).

The second dataset is that of Multiview Curve Dataset (MCD) proposed by Zuliani et al. [29], [30] and also used by [31]. This dataset consists of natural perspective deformations that a 2-D object could undergo. This dataset represent more realistic deformations than that of Dataset-I and it will be referred to as Dataset-II represented on Fig.16. The third dataset, called Dataset-III is extracted from the SQUID, presented and used in the studies conducted by F. Mokhtarian and M. Bober in [24] and by F. Mokhtarian et al. in [25]. The contours are selected so that the individuals from the same class are visually similar (see Fig.17). The fourth dataset, referred to as Dataset-IV, is based on that of the well-known MPEG-7 Core Experiments Shape-1. The goal of this experiment is to check robustness of a descriptor when facing deformations like scale change (Part A-1), rotation (Part A-2), and small non-rigid deformations (Part B). The last dataset is called Dataset-V. It is dedicated to the evaluation of retrieval systems relatively to non-rigid deformations due to motion. It is commonly referred to as Part C of the MPEG-7 Core Experiments Shape-1 (see Fig.18).

4.2 Performance assessment

In information retrieval, and particularly in CBIR (Content-Based Image Retrieval), there exist many measures to help evaluate a system. But as stated by Muller et al. in [32], it is most common to use the Recall and Precision curve to assess the performance of a retrieval system. Indeed, the Recall and Precision curve enables us to capture the global behavior of the system. Moreover, it may help to deepen the analysis by taken the Precision at a given number of retrieved patterns. The best system between two retrieval systems is that one whose curve is nearer to the upper-right corner of the graph. As indicated by Petrakis in [3], when two curves intersect, the best system is the one that gives higher Precision and higher Recall for large number of retrieved patterns: the right side of this curve must be above the other one.

Based on that statement, we plot Precision-Recall curves and then analyze the Bull's Eye Performance (BEP) [5] and the corresponding area under that curve (AUC) [33]. For this

purpose, each contour of the database is used as a query and then the first R most similar contours are retrieved. If RR is the number of retrieved relevant contours among the total of R retrieved contours, Precision and Recall are given by relations (14) and (15)

$$\text{Precision}(R) = \frac{\#(\text{Retrieved Relevant})}{\#\text{Retrieved}} = \frac{\text{RR}}{R} \tag{14}$$

$$\text{Recall}(R) = \frac{\#(\text{Retrieved Relevant})}{\#\text{Relevant}} = \frac{\text{RR}}{R_0} \tag{15}$$

where R_0 is the number of contours that are relevant to the query in the database.

The BEP corresponds to the Recall for the twice the number of relevant contours in the database (BEP=Recall($2R_0$)). The BEP and AUC parameters provide objective measures of the efficiency of a retrieval system. The higher they are the better is the system.

4.3 Evaluation on Dataset-I: marine animals

4.3.1 Description of the test set

To evaluate the ability of this d-TASS-based feature to discriminate objects, we have conducted retrieval experiments by applying our approach to a "synthetic" database of planar objects. Figure 11 shows the set of shapes of this database. As said before, this test set is drawn from the SQUID [28] database of marine animals contours. It is constructed by applying affine transformations to 50 original contours (see Fig.11). The transformation is defined by a composition of three transformations that are a rotation with rotation angle θ, a scaling with scale factor h and a shearing with a shearing factor λ. The affine transformation is then defined by:

$$\begin{pmatrix} x_o \\ y_o \end{pmatrix} = \begin{pmatrix} \cos(\theta) & -\sin(\theta) \\ \sin(\theta) & \cos(\theta) \end{pmatrix} \begin{pmatrix} h & 0 \\ 0 & h \end{pmatrix} \begin{pmatrix} 1 & \lambda \\ 0 & 1 \end{pmatrix} \begin{pmatrix} x_i \\ y_i \end{pmatrix} \tag{16}$$

where (x_i, y_i) are the coordinates of a point of the input contour and (x_o, y_o) the coordinates of the corresponding point of the transformed contour.

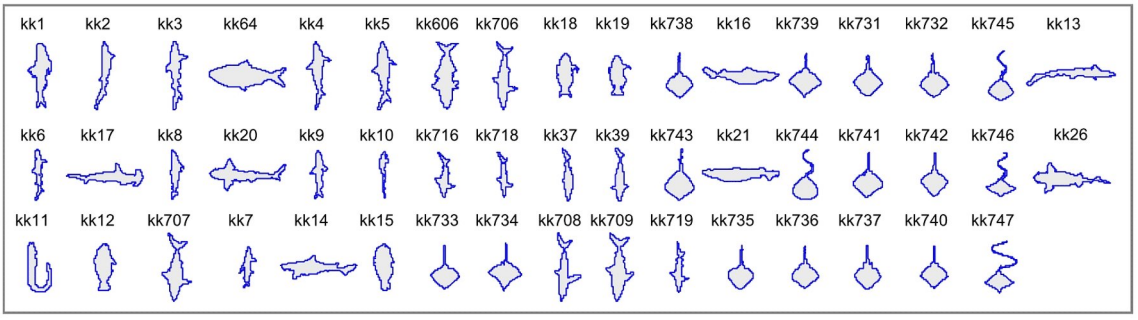

Fig.11: The 50 original contours selected from SQUID dataset

As mentioned in [1], we have defined three values referenced by n (n=0, 1, 2) for each parameter. Table II shows these parameters and their references. By using different combinations of these parameters, one can generate 27 transformed copies so that for each original contour, we have a family of 28 siblings. For this experiment, each original contour is different from the others so that for a given individual in the database, there are R_0=28 relevant shapes. Thus this test database consists of 50×28=1400 contours in total.

Figure 12, represents a contour (upper-left corner) and its siblings: the contour named

$R_xH_yL_z$kk1 is obtained from the original contour named kk1 after it has undergone rotation of angle θ_x, scaling factor h_y and shearing factor λ_z. For easier visualization, the contours have been rescaled to an appropriate size.

Table II: The set of affine transformation parameters

		Indices n of the parameters		
		0	1	2
Parameters	θ_n	45°	60°	90°
	h_n	0.25	0.75	5
	λ_n	0.3	0.6	1.5

The results presented in the next sections correspond to the average values all-over the database by using each of the 1400 contours as a query. Together with Table III, the graphs in figures 13 and 14 show the performance of the proposed features. This table shows the BEP and AUC for 16 different combinations of essential points and for four sizes of the feature matrix. In this table bold face values indicate BEP scores above 95%.

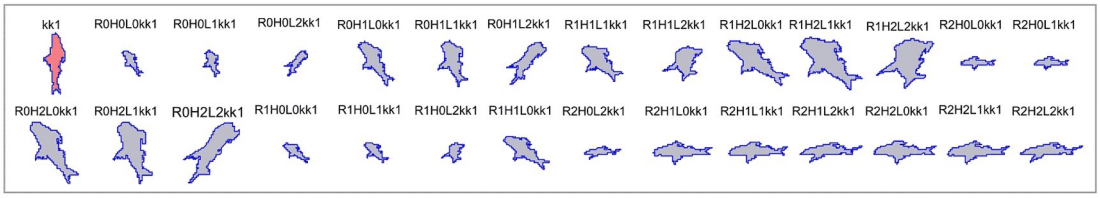

Fig.12: Example of a contour and its affine transforms.

4.3.2 Experimental results

In the experiments we have evaluated the effect of the size of the feature matrix and also the effect of the overlapping of the blocks. To evaluate the effect of the size of the feature matrix and as indicated previously, the d-TASS map is cut up into blocks of equal size. Prior to blocks generating, the d-TASS map has been circularly shifted to center the maximum peak of $\gamma-$points on the map. Figure 13 shows the Precision vs. Recall curves for different sizes (4×4, 8×8, 16×16, 32×32) of the feature matrix with 25% overlapping. For this experiment, the weights of essential points are set as follows: w_α=1, w_β=1 and w_γ=1.

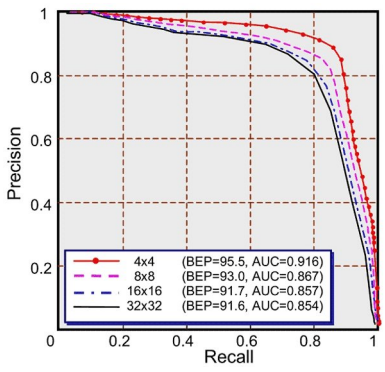

Fig.13: Example of Precision vs. Recall graphs.

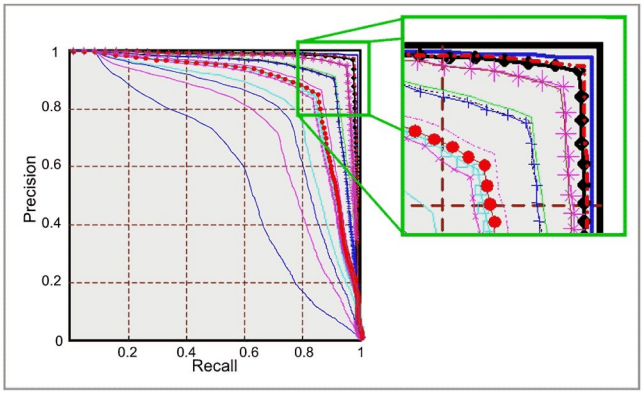

Fig.14: Precision vs. Recall graphs for 16 combinations of essential points in the case of 4×4 feature matrix with 25% overlapping.

As it can be seen on Figure 13, the feature matrix of size 4×4 gives the best performance, nevertheless, we must observe, thanks to Table III and Figure 14, that the performance depends not only on the size of the feature matrix but it also depends on the combination of the essential points.

To evaluate the overlapping effect, the overlapping rate is set to three values: 0, 25% and 50%. The majority of the experimental results showed 25% overlapping rate to give the best performance. One can observe up to 98.6% of BEP and 0.964 of AUC indicating high performance of the approach. This is confirmed by the Precision-Recall graphs that are close to the ideal case (upper-right corner of the figure, see the zoom of this corner on Figure 14).

Table III: Examples of retrieval performance

Essential pts weights	Performance parameter	Size of feature matrix M (25% overlapping blocks)			
$[w_\gamma\ w_\alpha\ w_\beta]$		4x4	8x8	16x16	32x32
[1 0 0]	BEP [%] (AUC)	**98.6 (0.964)**	**98.6 (0.963)**	**98.6 (0.963)**	**98.6 (0.963)**
[0 1 0]	BEP [%] (AUC)	88.7 (0.811)	92.6 (0.861)	**96.9 (0.921)**	**98.1 (0.946)**
[0 0 1]	BEP [%] (AUC)	75.8 (0.647)	66.9 (0.552)	69.7 (0.580)	72.0 (0.604)
[0 1 1]	BEP [%] (AUC)	84.5 (0.753)	79.3 (0.690)	81.4 (0.717)	84.0 (0.748)
[1 1 1]	BEP [%] (AUC)	**95.5 (0.916)**	93.0 (0.867)	91.7 (0.857)	91.6 (0.854)
[0.5 0.25 0.25]	BEP [%] (AUC)	**98.2 (0.953)**	**96.1 (0.922)**	**95.6 (0.911)**	**95.9 (0.909)**
[0.75 0.125 0.125]	BEP [%] (AUC)	**98.6 (0.964)**	**98.3 (0.959)**	**98.5 (0.957)**	**98.2 (0.951)**
[0.2 0.4 0.4]	BEP [%] (AUC)	91.9 (0.860)	87.9 (0.799)	87.6 (0.798)	88.5 (0.813)
[1 -1 1]	BEP [%] (AUC)	93.3 (0.893)	89.9 (0.833)	91.3 (0.846)	94.1 (0.879)
[1 -0.5 0.5]	BEP [%] (AUC)	**97.2 (0.942)**	**95.4 (0.910)**	**95.6 (0.909)**	**96.6 (0.919)**
[1 -0.25 0.25]	BEP [%] (AUC)	**98.2 (0.961)**	**97.5 (0.948)**	**97.6 (0.944)**	**97.9 (0.943)**
[1 1 -1]	BEP [%] (AUC)	93.8 (0.897)	91.5 (0.857)	92.5 (0.862)	93.5 (0.876)
[1 0.125 -0.125]	BEP [%] (AUC)	**98.6 (0.964)**	**98.6 (0.962)**	**98.5 (0.960)**	**98.2 (0.951)**
[1 0.25 -0.25]	BEP [%] (AUC)	**98.3 (0.960)**	**97.7 (0.949)**	**97.5 (0.943)**	**97.8 (0.940)**
[0.75 0.5 1]	BEP [%] (AUC)	91.1 (0.857)	85.6 (0.773)	85.0 (0.768)	86.0 (0.780)
[0.75 1 0.5]	BEP [%] (AUC)	94.8 (0.900)	93.5 (0.877)	93.0 (0,875)	93.8 (0.879)
Mean	BEP [%] (AUC)	93.6 (0.890)	91.4 (0.858)	91.9 (0.863)	92.8 (0.872)

From these experiments, we can observe that γ-points are very important: indeed, in most of the cases better performance is obtained when γ-points are weighted higher than the other essential points. It is also the most stable with respect to the size of the feature matrix because it gives almost the same performance for the tested sizes.

4.4 Evaluation on dataset-II: Multiview Curve Dataset (MCD)

This dataset consists of 40 shape classes drawn from the MPEG-7 Core Experiment Shape-1. Each class contains 14 contours corresponding to different perspective distortions of the original one. To construct the MCD dataset, the authors [34] have printed the 40 original contours on white paper. For each one, they took images from 7 different view angles using a digital camera and then contours are extracted. By adding random rotations and reflections to these samples, the number of samples in each class is doubled to 14. This dataset presents realistic perspective transformations that one can encounter while creating images of real objects. The performance of the descriptors is evaluated using the Precision-Recall curve averaged over the MCD.

The number R_0 of relevant contours is 14 for each class so the BEP corresponds to the Recall after 28 retrievals. The size of the feature matrix is set to 8×8, the weights applied to essential points are w_α=0.5, w_β=0.8 and w_γ=1.5 and those applied to moment matrices are a_{00}=4, a_{01}=2, a_{10}=2 and a_0=4. Figure 15 illustrates the Precision vs. Recall graph. The curve plotted on this graph sticks to the upper side and the right side of the figure (very close to the upper-right corner) indicating high performance system.

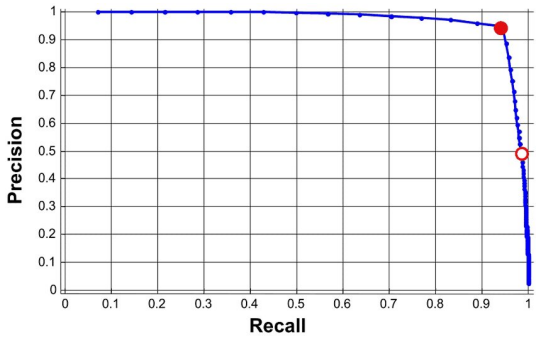

Fig.15 Mean Precision-Recall curve

On this graph, the point • corresponds to Recall and Precision after 14 retrievals while the point ∘ corresponds to the BEP. On this curve, one can observe that after having retrieved 14 contours, the Precision and Recall are higher than 94.5%. This shows that the proposed method outperforms that of HCD [29] that reports a precision of 85% for a recall of 86%. The performance reported in a recent study, conducted on the same dataset, by Ekombo et al. [31] is not more than 90% Precision for 90% Recall.

Figure 17 shows a sample set of retrieval results. The first column is the query and the middle indicates the 14 most similar contours. Mis-classified shapes are represented with different color (say red edge and yellow foreground). The similarity score is decreasing when going from left to right. The last column is the ratio of the retrieved relevant to the number of relevant contours in the class. As can be seen, apart from bird01 and bottle01, all the queries have provided a precision of 100% after 14 retrievals. This confirms the high BEP rate obtained and the behavior of the Precision-Recall curve presented in figure 15. Moreover, one must also notice that in the cases of less than 100% precision, mis-retrieved shapes appear at the last positions corresponding to the lowest similarity score.

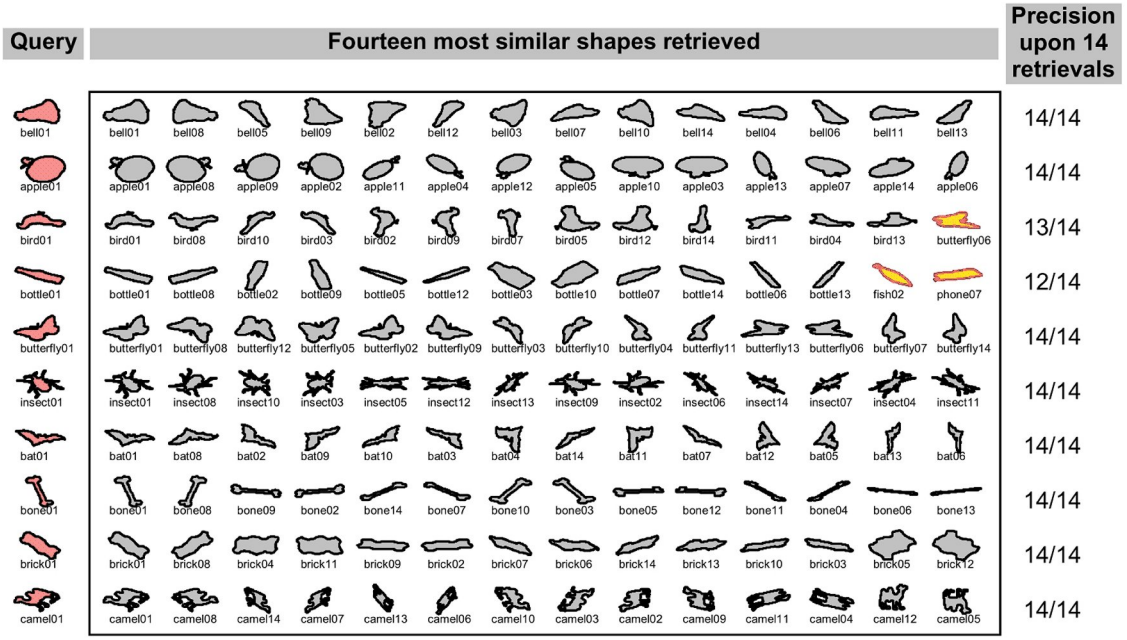

Fig.16: A sample of retrieved contours: first column is the query, middle is 14 most similar and last column is the ratio of the retrieved relevant over the number of relevant contours in the class.

4.5 Evaluation on Dataset-III: marine animals

This dataset consists of 17 classes containing from 6 to 8 objects selected from the marine animals of SQUID database. For comparison, we have followed the same procedure proposed and used by the author of the database [25] and [26]. This procedure is similar to the concept of Recall presented previously: thus the performance that is used corresponds to the BEP. The procedure is as follows:

1. For a given class, use each of the contours as the query and determine the first 15 most similar outputs. Within these 15 outputs, count the number of relevant contours that are retrieved and compute the ratio of this number to the number of relevant contours in the class. Repeat this for all contours in the considered class. The mean value of this ratio all-over the class is the performance measure for the concerned class (see individual columns in table IV).
2. Repeat 1. for all the classes in the dataset. The overall performance is then obtained by averaging the performance provided by the 17 classes. Column 'Overall' in table IV, gives that overall performance for the four involved methods.

To assess the performance of the proposed method, its results are compared to those obtained from three methods tested on the same database and reported in [24]. These compared methods are the well-known CSS, the Fourier descriptor (FD) and the moment invariants (MI).

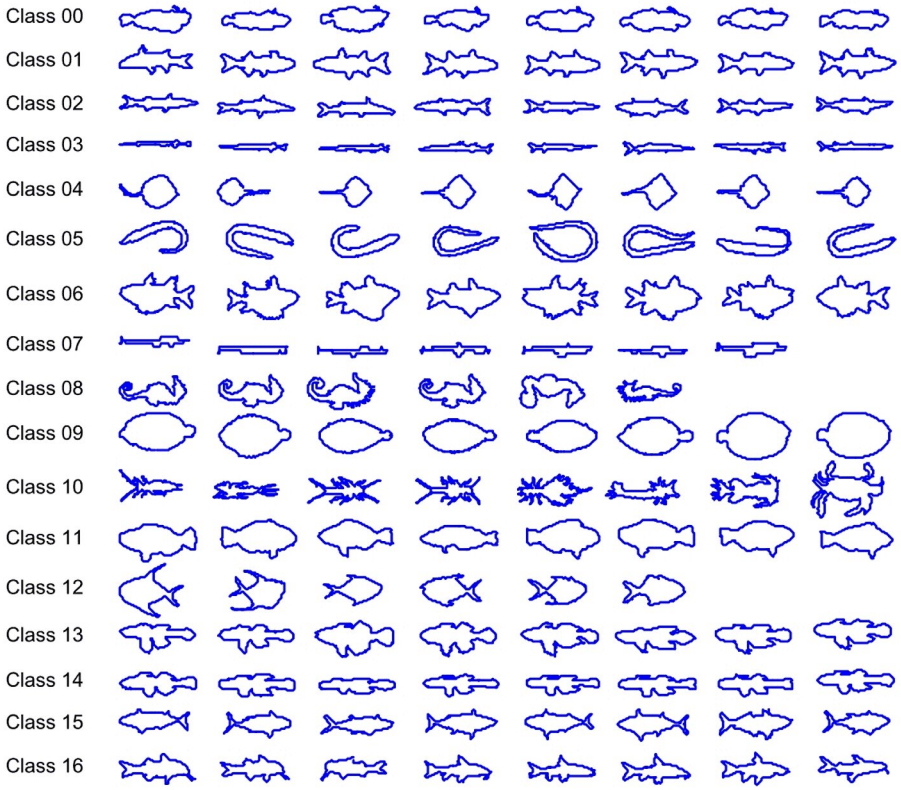

Fig.17: Dataset-III extracted from the SQUID database

For this experiment, the size of the feature matrix is set to 8×8 with 25% overlapping. The weights applied to essential points are w_α=1.5, w_β=1.25 and w_γ=1.25 and those applied to moment matrices are a_0=1, a_{01}=0.5, a_{10}=0.5 and a_0=1. Regarding table IV, one can notice that the proposed method ranks the second with 87% performance after CSS method.

Table IV: Comparison of retrieval performance for four methods

	Class N°	1	2	3	4	5	6	7	8	9	10	11	12	13	14	15	16	17	**Overall**
Descriptors	CSS	89	86	81	95	100	100	91	98	75	92	81	100	94	89	100	95	69	**91**
	d-TASS	**81**	**98**	**84**	**91**	**100**	**95**	**72**	**92**	**83**	**100**	**73**	**97**	**100**	**36**	**100**	**97**	**78**	**87**
	FD	100	84	100	75	78	42	80	100	36	98	13	70	78	98	73	97	48	**75**
	MI	34	78	91	100	88	41	72	86	47	53	23	91	53	45	72	73	58	**65**

4.6 Evaluation on MPEG-7 datasets

The proposal is also compared with various recent methods reported in the literature [12], [35], [14] and [20]. This will enable us to evaluate our approach relatively to studies of the state-of-the-art.

The following datasets from MPEG-7 are used to evaluate the retrieval system. Traditionally, the evaluation is reported individually on each Part and then the global score is computed: the results are presented in table V. For the following experiments, the size of the feature matrix is set to 10×11 with 25% overlapping. The weights applied to essential points are w_α=0.8, w_β=0.5 and w_γ=0.8 and those applied to moment matrices are a_{00}=4.8, a_{01}=2.6, a_{10}=2 and a_0=1.6.

4.6.1 Evaluation on Dataset-IV: MPEG-7 CE-Shape-1

The whole database is composed of 1400 contours classified into 70 classes containing 20 visually similar contours each. Within-class deformations include occultation and non-rigid deformations. This experiment aims at the evaluation of 2-D shape descriptors when the shape has undergone change of viewpoint, non-rigid motion and noise. The experiments are then conducted according to following three parts:

Part A-1 is dedicated to evaluate the robustness of the descriptor against scale change. The dataset used for this experiment is composed of 70 basic shapes selected from the original dataset-IV. Then each of them is scaled with 5 scale factors: S=[2.0 0.3 0.25 0.2 0.1]. This leads to 420 individuals in the dataset with 6 individuals in each class. Each individual is used as a query and the number of correct matches is computed in the Top-6 contours. The success rate is reported on the row Part A1 of Table V. The proposed method gives 100% success rate, outperforming all other methods.

Part A-2 is utilized to evaluate the robustness of the descriptor against rotation. Like for Part A-1, the test set is composed of 70 basic shapes selected from the original Dataset-IV. Each of them is rotated by using 5 angles: R=[9 36 45 90 150]. Again, this leads to 420 objects in the dataset with 6 individuals in each class. The same way, each individual is used as a query and the number of correct matches is computed in the Top-6 contours. The retrieval success rate is reported on the row Part A2 of Table V. Again ; the proposed method gives 100% success rate, outperforming all other methods.

Part B is the similarity-based retrieval and it is the most difficult part. The whole dataset-IV is used. Each of the 1400 shapes is used as query and the number of relevant objects retrieved in the Top-40 is computed. This value corresponds to the BEP. Recently, Bandera et al. have proposed a new description approach based on an adaptive curvature estimator by using a global incremental scheme in [7]. Experiments conducted using the MPEG-7 CE-shape-1 Part B showed good performance in terms of BEP. Table V shows the BEP performance of various shape description techniques reported in the state of the art (see row Part B). The proposed method gives 76.92% BEP.

4.6.2 Evaluation on Dataset-V: video clip of marine animals

Commonly referred to as Part C, it concerns a test to assess the performance of the retrieval system when facing motion and non-rigid deformations. The dataset is composed of contours extracted from 200 frames of a video clip of a swimming bream fish plus 1100 contours of marine animals. Fig.18 shows a sample set of the video clip. The contour of the bream fish named "bream-000" is then used as query and the number of relevant objects retrieved in the Top-200 is computed. This way, the maximum number of possible matches is 200. The retrieval success rate is reported on the row Part C of Table V. As opposed to what is said by Latecki et al. in [20], this table shows that some descriptors give more than 93% accuracy in Part C. With our method, this accuracy equals 93.53%.

Fig.18: The query shape (bream-000) and a sample set of the bream fish video.

4.6.3 Comparison and discussion of the results

In order to get a global quantitative measurement to compare these different methods, we use the mean retrieval performance obtained by combining the performance rates computed for the three parts. The accuracy assessment is done relative to two average values as suggested by Latecki et al. in [20] and also used by Mokhtarian et al. in [24] (see equations (17) and (18)).

- MeanScore_1 defined by the average performance over the three parts:

$$\text{MeanScore}_1 = \frac{0.5(\text{PartA1} + \text{PartA2}) + \text{PartB} + \text{PartC}}{3} \tag{17}$$

- MeanScore_2 defined by the average over the number of queries 2241 queries:

$$\text{MeanScore}_2 = \frac{420\text{PartA1} + 420\text{PartA2} + 1400\text{PartB} + \text{PartC}}{2241} \tag{18}$$

Table V, shows the comparison of the proposed method with some recent studies reported in the literature [35]. All the papers involved in this study report a value for Part B but not all of them report Part A and Part C. Hence the comparison will be assessed onto two groups based on two aspects according to the available measurement.

Table V: Comparison of the results obtained from different methods reported in the literature

		Descriptors														
Data set		WARP	VP	SC	CED	MCC	Bandera	IDSC	TA-DSW	DAG	Wavelet	ZM	CSS	TS	BAS	d-TASS 10x11
	Part A1	-	88.65	-	-	-	-	-	98.02	85	88.04	92.54	89.76	88.65	90.87	**100**
	Part A2	-	100	-	-	-	-	-	100	85	97.46	99.60	99.37	100	100	**100**
	Part B	58.50	76.45	76.51	78.17	84.93	84.97	85.40	87.23	60	67.76	70.22	75.44	76.45	82.37	**76.92**
	Part C	-	-	-	-	-	-	-	-	83	93	94.50	96	92	93.50	**93.53**
Mean Scores	$MeanScore_1$	-	-	-	-	-	-	-	-	76	84.50	86.93	88.67	87.59	90.44	**90.15**
	$MeanScore_2$	-	-	-	-	-	-	-	-	69.38	77.14	79.92	82.62	83.16	87.27	**85.58**

The first group is concerned with Part B: in this category, fifteen methods are available. As can be seen on this table, our proposed method is the 7^{th} best among the 15 presented methods. It presents a BEP score of 76.92% face to 87.23% for the highest (TA-DSW [11]) and 58.5% for the lowest (WARP [16]).

Recently, Ahmad et al. have introduced an approach similar to TA-DSW which gave 86.65% of BEP. It is a hybrid approach that uses both interior region and shape contours features: the descriptor consists of a set of local contour-based and region-based features extrated from the labeled grid representation of the shape.

The second group consists of seven methods that report all the measurements involved in the computation of MeanScore1 and $MeanScore_2$. For both scores, the proposed method is the second; using the first type score ($MeanScore_1$), the proposed method obtains a score of 90.15% behind but very close to the best score of 90.44% (for BAS-60 [14]). The lowest score in this category is 76% for DAG [22].

5. Conclusion

The context of this paper is the description of planar objects based on the multi-scale analysis of their contours. For this purpose, we have presented and tested a new feature extracted from the d-TASS map. The proposed descriptor is derived from a matrix generated by weighted moments extracted from blocks within the d-TASS map. As for other multi-scale approaches, one of the advantages of this descriptor holds in its ability to integrate information from multiple scales at the same time.

The main contribution of this paper is the extensive experiments conducted on various datasets to compare the proposed approach with other methods proposed in the literature.

Experiments show that the proposed approach ranks 2^{nd} on SQUID database and outperforms other methods on MCD dataset.

When applied to shape retrieval from MPEG-7 CE-Shape-1 databases, the obtained results show that this d-TASS-based descriptor is very promising: up to 93.53% performance is reached in case of deformations due to motion, on Part C. Although the results of 93.32% of BEP on Part B, presented by a recent study [36] outperforms the proposed method, one can notice its satisfactory performance over the same dataset. It is particularly interesting to notice that the proposed method outperforms a recent performance of 76.56% reported in [37] on Part B. Especially, one must highlight the 100% performance obtained from this method when applied to Part A-1 and Part A-2 datasets: this confirms the perfect insensitivity of the method to rotation and scaling. The main weakness of the proposal is the large number of parameters so one may consider another combination of d-TASS features in order to reduce this number.

In terms of global mean score, the proposed method holds a honorable rank among the well-established methods since it is ranked second among the seven presented methods.

Though the proposed method provides average performance when applied to MPEG-7 Part B, it offers satisfactory and encouraging results when we analyze the results obtained from various datasets.

To improve the proposed approach, failure cases need to be analyzed more deeply: this will allow to better adjust the parameters properly to make them be more generic for all datasets. So, future work will mainly focus on the analysis of failure cases in each dataset and then set optimal values for the parameters.

Acknowledgments

This work is partially supported by the Franco-Algerian Programme "Partenariat Hubert-Curien PHC-TASSILI" under grant No 12MDU864. The authors thank for their fanancial support

References

[1] K. Kpalma, M. Yang, and J. Ronsin, "Planar shapes descriptors based on the turning angle scalogram," in *Proceedings of the 5th International Conference on Image Analysis and Recognition*, ICIAR '08, (Berlin, Heidelberg), pp. 547–556, Springer-Verlag, 2008.

[2] K. Kpalma and J. Ronsin, "Turning angle based representation for planar objects," *Electronics Letters*, vol. 43, pp. 561–562, May 2007.

[3] E. G. M. Petrakis, A. Diplaros, and E. Milios, "Matching and retrieval of distorted and occluded shapes using dynamic programming," *IEEE Trans. Pattern Anal. Mach. Intell.*, vol. 24, pp. 1501–1516, Nov. 2002.

[4] K. Kpalma and J. Ronsin, "An overview of advances of pattern recognition systems in computer vision," in *Vision Systems : Segmentation and Pattern Recognition* (G. Obinata and A. Dutta, eds.), ch. 10, InTech, 2007.

[5] G. McNeill and S. Vijayakumar, "2d shape classification and retrieval," in *Proceedings of the 19th International Joint Conference on Artificial Intelligence*, IJCAI'05, (San Francisco, CA, USA), pp. 1483–1488, Morgan Kaufmann Publishers Inc., 2005.

[6] D. Zhang and G. Lu, "Review of shape representation and description techniques," *Pattern Recognition*, vol. 37, no. 1, pp. 1–19, 2004.

[7] Y. S. Avrithis, Y. Xirouhakis, and S. D. Kollias, "Affine-invariant curve normalization for object shape representation, classification, and retrieval.," *Mach. Vis. Appl.*, vol. 13, no. 2, pp. 80–94, 2001.

[8] K. Kpalma and J. Ronsin, "Multiscale contour description for pattern recognition.," *Pattern Recognition Letters*, vol. 27, no. 13, pp. 1545–1559, 2006.

[9] M. Yang, K. Kpalma, and J. Ronsin, "Affine invariance contour descriptor based on iso-area normalization," *IEE Electronics Letters*, 2007.

[10] D. Zhang and G. Lu, "Evaluation of similarity measurement for image retrieval," in *Neural Networks and Signal Processing, 2003. Proceedings of the 2003 International Conference on*, vol. 2, pp. 928–931 Vol.2, Dec 2003.

[11] N. Alajlan, I. El Rube, M. S. Kamel, and G. Freeman, "Shape retrieval using triangle-area representation and dynamic space warping," *Pattern Recogn.*, vol. 40, pp. 1911–1920, July 2007.

[12] J. Ahmad, Z. Jan, Z. U. Din, and S. M. Khan, "A fusion of labeled-grid shape descriptors with weighted ranking algorithm for shapes recognition," *CoRR*, vol. abs/1406.3949, 2014.

[13] T. Adamek and N. O'Connor, "A multiscale representation method for nonrigid shapes with a single closed contour," *Circuits and Systems for Video Technology, IEEE Transactions on*, vol. 14, pp. 742–753, May 2004.

[14] N. Arica and F. T. Yarman-Vural, "Bas : a perceptual shape descriptor based on the beam angle statistics.," *Pattern Recognition Letters*, vol. 24, no. 9-10, pp. 1627–1639, 2003.

[15] A. Bandera, R. Marfil, and E. Antunez, "Affine-invariant contours recognition using an incremental hybrid learning approach.," *Pattern Recognition Letters*, vol. 30, no. 14, pp. 1310–1320, 2009.

[16] I. Bartolini, P. Ciaccia, and M. Patella, "Warp : Accurate retrieval of shapes using phase of fourier descriptors and time warping distance," *IEEE Trans. Pattern Anal. Mach. Intell.*, vol. 27, pp. 142–147, Jan. 2005.

[17] S. Belongie, J. Malik, and J. Puzicha, "Shape matching and object recognition using shape contexts," *Pattern Analysis and Machine Intelligence, IEEE Transactions on*, vol. 24, pp. 509 –522, Apr. 2002.

[18] G. C.-H. Chuang and C. C. J. Kuo, "Wavelet descriptor of planar curves : theory and applications.," *IEEE Transactions on Image Processing*, vol. 5, no. 1, pp. 56–70, 1996.

[19] A. Khotanzad and Y. H. Hong, "Invariant image recognition by zernike moments.," *IEEE Trans. Pattern Anal. Mach. Intell.*, vol. 12, no. 5, pp. 489–497, 1990.

[20] L. Latecki and R. Lakamper, "Shape similarity measure based on correspondence of visual parts," *Pattern Analysis and Machine Intelligence, IEEE Transactions on*, vol. 22, pp. 1185–1190, Oct 2000.

[21] L. Latecki, R. Lakamper, and T. Eckhardt, "Shape descriptors for non-rigid shapes with a single closed contour," in *Computer Vision and Pattern Recognition, 2000. Proceedings. IEEE Conference on*, vol. 1, pp. 424–429 vol.1, 2000.

[22] I.-J. Lin and S. Y. Kung, "Coding and comparison of dags as a novel neural structure with applications to on-line handwriting recognition," in *IEEE Transactions on Signal Processing*, 1997.

[23] H. Ling and D. Jacobs, "Using the inner-distance for classification of articulated shapes," in *Computer Vision and Pattern Recognition, 2005. CVPR 2005. IEEE Computer Society Conference on*, vol. 2, pp. 719–726 vol. 2, June 2005.

[24] F. Mokhtarian and M. Bober, *Curvature Scale Space Representation : Theory, Applications and MPEG-7 Standardization.* Kluwer Academic, 2003.

[25] F. Mokhtarian, S. Abbasi, and J. Kittler, "Efficient and robust retrieval by shape content through curvature scale space," 1996.

[26] F. Mokhtarian and A. Mackworth, "A theory of multiscale, curvature-based shape representation for planar curves," *Pattern Analysis and Machine Intelligence, IEEE Transactions on*, vol. 14, pp. 789–805, Aug 1992.

[27] T. Sebastian, P. Klein, and B. Kimia, "On aligning curves," *Pattern Analysis and Machine Intelligence, IEEE Transactions on*, vol. 25, pp. 116–125, Jan 2003.

[28] "http ://www.ee.surrey.ac.uk/cvssp/demos/css/demo.html, accessed november 25, 2010," 2010.

[29] M. Zuliani, L. Bertelli, C. S. Kenney, S. Chandrasekaran, and B. S. Manjunath, "Drums, curve descriptors and affine invariant region matching," *Image Vision Comput.*, vol. 26, pp. 347–360, Mar. 2008.

[30] "http ://vision.ece.ucsb.edu/ zuliani/research/mcd/mcd.shtml, accessed november 25, 2010," 2010.

[31] P. L. E. Ekombo, N. Ennahnahi, M. Oumsis, and M. Meknassi, "Application of affine invariant fourier descriptor to shape-based image retrieval," *IJCSNS International Journal of Computer Science and Network Security*, vol. 9, July 2009.

[32] H. Müller, W. Müller, D. M. Squire, S. Marchand-Maillet, and T. Pun, "Performance evaluation in content-based image retrieval : Overview and proposals," *Pattern Recogn. Lett.*, vol. 22, pp. 593–601, Apr. 2001.

[33] H.-Y. Lo, C.-M. Chang, T.-H. Chiang, C.-Y. Hsiao, A. Huang, T.-T. Kuo, W.-C. Lai, M.-H. Yang, J.-J. Yeh, C.-C. Yen, and S.-D. Lin, "Learning to improve area-under-froc for imbalanced medical data classification using an ensemble method.," *SIGKDD Explorations*, vol. 10, no. 2, pp. 43–46, 2008.

[34] M. Zuliani, S. Bhagavathy, B. Manjunath, and C. Kenney, "Affine-invariant curve matching," in *Image Processing, 2004. ICIP '04. 2004 International Conference on*, vol. 5, pp. 3041–3044 Vol. 5, Oct 2004.

[35] F. A. Andalo, P. A. V. Miranda, R. da Silva Torres, and A. X. Falcao, "Shape feature extraction and description based on tensor scale.," *Pattern Recognition*, vol. 43, no. 1, pp. 26–36, 2010.

[36] X. Yang, S. Koknar-Tezel, and L. Latecki, "Locally constrained diffusion process on locally densified distance spaces with applications to shape retrieval," in *Computer Vision and Pattern Recognition, 2009. CVPR 2009. IEEE Conference on*, pp. 357–364, June 2009.

[37] X. Shu and X.-J. Wu, "A novel contour descriptor for 2d shape matching and its application to image retrieval," *Image and Vision Computing*, vol. 29, no. 4, pp. 286 – 294, 2011.